FLUTTER SUPPRESSION FOR THE ACTIVE FLEXIBLE WING: CONTROL SYSTEM DESIGN AND EXPERIMENTAL VALIDATION

AIAA-92-2097-CP

M.R. Waszak, *NASA Langley Research Center, Hampton, Virginia* *
Dr. S. Srinathkumar, *National Aeronautical Laboratory, Bangalore, India* **

Abstract

The synthesis and experimental validation of a control law for an active flutter suppression system for the Active Flexible Wing wind-tunnel model is presented. The design was accomplished with traditional root locus and Nyquist methods using interactive computer graphics tools and with extensive use of simulation-based analysis. The design approach relied on a fundamental understanding of the flutter mechanism to formulate a simple control law structure. Experimentally, the flutter suppression controller succeeded in simultaneous suppression of two flutter modes, significantly increasing the flutter dynamic pressure despite errors in the design model. The flutter suppression controller was also successfully operated in combination with a rolling maneuver controller to perform flutter suppression during rapid rolling maneuvers.

Introduction

Modem aircraft designs emphasize the reduction of structural weight to maximize efficiency and agility. Reduced structural weight. however. can result in reduced stiffness and may increase the likelihood of structural dynamic instabilities (flutter). Active flutter suppression is a possible solution to dynamic problems associated with reduced weight. Developing methods to suppress flutter by utilizing active control systems was one objective of the Active Flexible Wing (AFW) program [Perry, Cole and Miller **(1992)).**

This paper focuses on the design and wind-tunnel test of a control law for an active flutter suppression system (FFS). The operation of the flutter suppression controller with the AFW wind-tunnel model in a fixed attitude and while performing rapid rolling maneuvers are specifically addressed. An emphasis is placed on developing an understanding of the fundamental dynamic characteristics of the flutter mechanism and employing feedback in a manner that stabilizes the flutter mode without otherwise adversely affecting the basic dynamic properties of the wind-tunnel model and without undue complexity. Additional discussion of the design and validation of the control laws described herein is presented in Waszak and Srinathkumar (1991) and Waszak and Buttrill (1991).

Wind-Tunnel Model Flutter Characterization

Experimental Facilities

The AFW wind-tunnel model was an actively controlled, statically and aeroelastically scaled. full-span wind-tunnel model of an advanced fighter aircraft. The vehicle was supported by a sting with a ball bearing and brake mechanism that allowed the vehicle to be fixed or free to roll about the sting axis. Four control surfaces, controlled by hydraulic actuators, were located on each wing semispan: leading edge outboard (LEO), leading edge inboard (LEI), trailing edge outboard (TEO), and trailing edge inboard (TEI). Only three of these surfaces (LEO, TEI. and TEO) were utilized for flutter suppression. Four accelerometers were located on each wing semispan. Three of the accelerometers were located near the hingelines of the LEO. TEO and TEI control surfaces near the surface midspan and one was located near the wingtip at about midchord. A more detailed description of the wind-tunnel model is presented in Perry, Cole and Miller **(1992).**

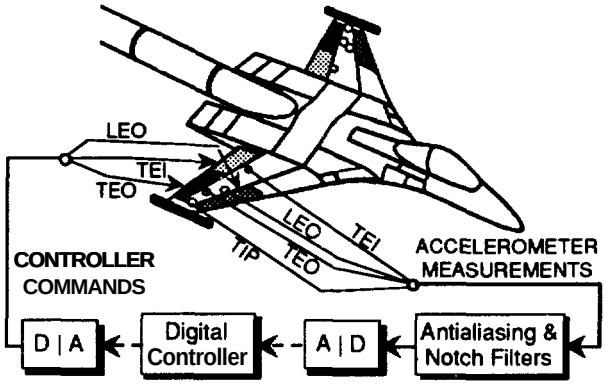

Figure 1 AFW wind-tunnel model and controller.

The active flutter suppression control law was implemented on a digital computer running at 200 samples per second. Analog measurement signals were prefiltered by a first-order. 25 Hertz antialiasing filter and could also be passed through notch filters. A schematic diagram of the AFW wind-tunnel model and controller is depicted in Figure 1. A detailed description of the digital controller is presented in Hoadley and McGraw **(1992).** The controller structure shown in Figure 1 could not be modified by the control law designer other than to specify characteristics of analog notch filters. Analog notch filters were not required for the control law described herein.

The wind-tunnel model and digital controller were tested during two wind-tunnel entries. These tests were performed in the NASA Langley Transonic Dynamics Tunnel (TDT). The operating conditions were limited to low subsonic speeds (< Mach **0.5)** at atmospheric pressure. Dynamic pressure was varied over a range from 0 to approximately 300 psf.

Mathematical Model

A high-fidelity simulation model of the AFW wind-tunnel model was used for control law synthesis and analysis. It consisted of representations of structural and aerodynamic characteristics. control surface actuator dynamics, wind-tunnel turbulence, and digital controller dynamics. Linear equations of motion for the structural dynamics, unsteady aerodynamics. and controller dynamics were used. but nonlinearities such as control surface deflection limits. actuator rate limits. and quantization effects were also characterized. The effects of wind-tunnel turbulence were incorporated into the model using an appropriately calibrated Dryden spectrum representation. A detailed description of the mathematical model can be found in Buttrill. et al. **(1992)** and Buttrill and Houck **(1990).** Linear models, used extensively in the control system design and analysis process, were obtained by linearizing the nonlinear model about equilibrium points at various operating conditions.

Flutter Mechanism

The predicted symmetric and antisymmetric dynamic characteristics of the AFW wind-tunnel model fixed in roll are summarized by the dynamic pressure root loci presented in Figures 2 and 3. The root loci describe the variation in pole and zero locations with variations in dynamic pressure of the open-loop transfer function associated with symmetric and antisymmetric tip accelerometer responses due to TEO actuator

* Aerospace Research Engineer, Member AIAA.
** Senior National Research Council Associate, NASA Langley Research Center. National Aeronautical Laboratory, Bangalore, India.

commands. Figures 2(a) and 3(a) depict the loci of the symmetric and antisymmetric structural modes contained in the model. respectively. Figures 2(b) and 3(b) depict close-ups of the flutter regions. The symmetric loci are the same regardless of whether the model is fixed in roll or free to roll. Only symmetric flutter occurred within the operating range of the wind-tunnel when the model was free to roll.

While fixed in roll, the AFW wind-tunnel model exhibited two distinct flutter modes (symmetric and antisymmetric) within the operating range of the wind-tunnel. There were obvious similarities between the shape of the dynamic pressure root locus paths for the symmetric and antisymmetric flutter mechanisms. These are evident by comparing the root loci in the flutter region in Figures 2(b) and 3(b). The mathematical model predicted that the flutter modes had similar flutter frequencies (symmetric - 11.2 Hertz, antisymmetric - 10.9 Hz) and similar flutter dynamic pressures (symmetric - 248 psf, antisymmetric - 233 psf).

Analysis of the mathematical model predicted that the AFW wind-tunnel model exhibited classical wing bending/torsion flutter [Bisplinghoff and Ashley (1975)]. The flutter modes were characterized by coupling between the first wing bending mode and the first wing torsion mode. At low dynamic pressures these two modes were distinct from each other with characteristic bending and torsion mode shapes. As the dynamic pressure increased. these two modes became coupled so that the bending and torsion modal frequencies coalesced to a common frequency and took on mode shapes that exhibited characteristics of both wing bending and wing torsion. Eventually. one mode became unstable and manifested itself as a divergent oscillation.

Characteristics of the root loci in Figures 2 and 3 played a key role in suppressing the flutter modes. The root loci indicate a distinct frequency separation between the modes that participated in the transition to flutter and the modes associated with higher frequency structural modes and unsteady aerodynamics. This implies that the FSS should be able to stabilize the flutter modes without significantly affecting. or being affected by, higher order dynamics. However, potential interactions could occur with a secondary symmetric flutter mode (see Figure 2(a)) which occurred at a frequency of approximately 35 Hertz (much higher than the primary flutter mode) and which became unstable at a dynamic pressure well above that of the primary flutter mode.

Control Law Development

Design Objectives, Specifications, and Approach

The primary performance objective of the flutter suppression control law was to maintain stability over the range of dynamic pressures that were anticipated during the wind-tunnel tests (0 - 300 psf) subject to the disturbances associated with nominal wind-tunnel turbulence. An additional objective was to perform rapid rolling maneuvers while simultaneously performing flutter suppression. This required the concurrent operation of both an FSS controller and a rolling maneuver controller.

Specifications were developed to reflect required levels of robustness. Gain and phase margins of ±4 dB and ±30 degrees. respectively, (or their multivariable equivalents) were required over the operating range to account for modeling errors and uncertainties. To reduce the probability of rate limiting the control surface actuators, the RMS commanded actuator rate was required to be less than one third the maximum achievable rate, about 50 degrees per second in this case.

Since the controller had to operate at a sampling rate of 200 Hertz, the control law had to be simple enough that all required computations could be completed in a fraction of the sample period of 0.005 second. This was particularly crucial when simultaneously performing flutter suppression and roll control since the same digital controller had to perform both functions.

The basic design philosophy for the FSS control law was to devise the simplest control law structure that met all the design objectives. A low complexity control law increased the likelihood of meeting computational requirements. It also

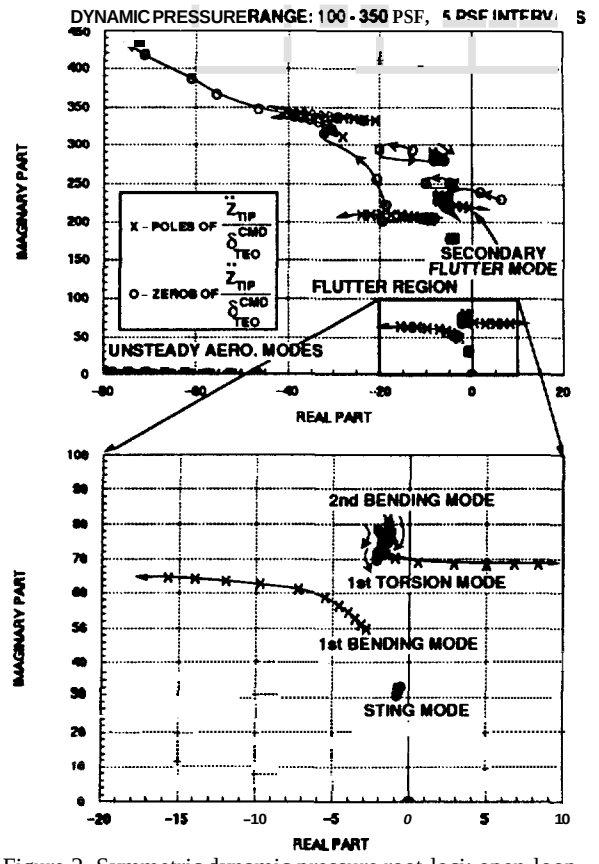

Figure 2 Symmetric dynamic pressure root loci: open-loop.

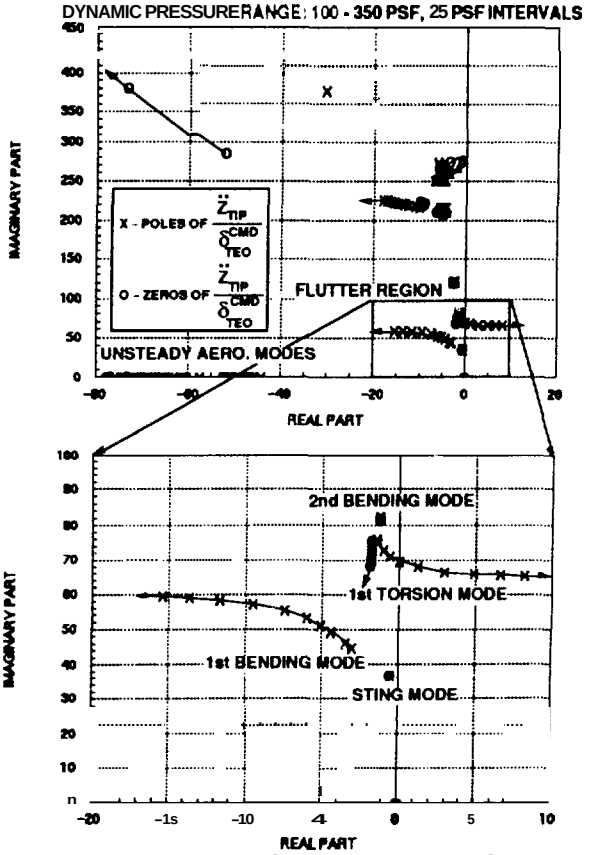

Figure 3 Antisymmetric dynamic pressure root loci: open-loop (roll brake on).

allowed the designer to retain the ability to readily identify the relationships between the open-loop system dynamics and the effects of feedback. The design approach was to first reduce the number of sensors and control surfaces required to suppress the flutter and then identify a simple compensation strategv to satisfy the design specifications.

Choice of Sensors and Control Surfaces

To simplify the control law synthesis, only the control surfaces that were most effective in controlling the flutter modes and only those sensors most able to sense the flutter motion were chosen. Predictions indicated that the trailing edge inboard and outboard surfaces were much more effective in controlling both symmetric and antisymmetric flutter than the leading edge surface. The TEO surface was predicted to be effective in controlling the symmetric and antisymmetric first wing bending modes while the TEI surface was predicted to be effective in controlling the antisymmetric first wing torsion mode. Therefore, only the TEO surfaces were considered for suppressing the symmetric flutter mode and the two pairs of trailing edge surfaces (TEO and TEI) were considered for suppressing the antisymmetric flutter mode.

The predicted accelerometer characteristics were such that, while each accelerometer was fairly responsive to the flutter modes, only the wingtip accelerometer demonstrated desirable high frequency roll-off The LEO. TEI, and TEO accelerometers were sensitive to high frequency modes and would have required additional filtering to generate the required high frequency roll-off. The phase lags and the added complexity associated with additional filtering were deemed undesirable. As a result, the wingtip accelerometer ($\ddot{z}_{TIP}$) was the only sensor used in the design.

Control Law Synthesis

The control law synthesis process was similar to that used by Schmidt and Chen (1986). The basic tools used in the FSS design process were root locus and Nyquist plots. The control law was designed as a continuous time system and discretized using the Tustin transformation. The discretization process is described in Waszak and Buttrill (1991). Analyses of the AFW/FSS system were performed using both the high-fidelity nonlinear simulation model and simplified linear models to address performance and robusmess issues. The simulation model was used whenever nonlinearities were suspected to have a potential impact.

The first step in the synthesis procedure was to assess the potential for simple constant gain feedback (without additional compensation) to stabilize the flutter modes. This was accomplished by considering the symmetric flutter mode with the model fixed-in-roll. The objective was not necessarily to use constant gain feedback exclusively in the final design, but to develop insight into the control mechanism and assess the problems that would likely occur in attempting to employ a simple solution.

Inspection of the open-loop dynamic pressure root loci for the wingtip acceleration due to TEO surface deflection, Figures 2(a) and 3(a), reveals that the flutter mechanism depended primarily on two structural modes. These modes, their associated zeros, and the two zeros at the origin associated with the use of acceleration feedback were all that was required to effectively characterize the flutter mechanism. Two additional modes in the same frequency range (sting mode and second bending mode) had little influence since, for the chosen sensor-actuator combinations, there were near pole–zero cancellations associated with these modes. The large frequency separation between the flutter region and the other vehicle dynamics allowed the higher order dynamics to be neglected during the design process. However, the potential impact of the neglected dynamics on system performance were considered during the design process.

The idealized pole-zero constellation depicted in Figure 4 corresponds to a dynamic pressure above that of open-loop flutter. Two gain root loci can result when attempting to stabilize this system with constant gain feedback. One locus is

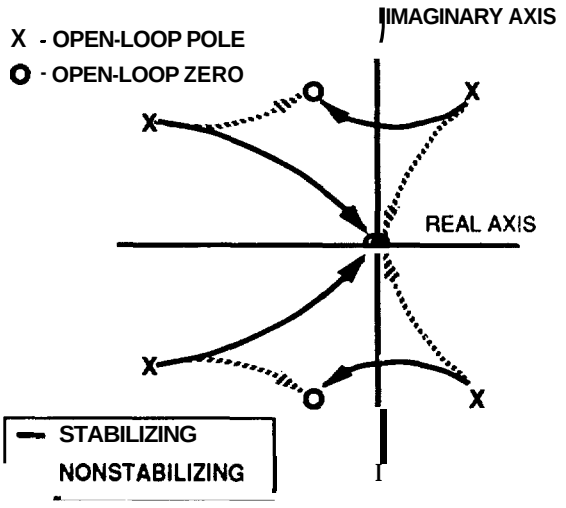

Figure 4 Two possible gain root loci.

stabilizing and the other is nonstabilizing. Which of the two loci occurs depends on the relative position of the poles and zeros of the subject transfer function. The control law must produce a stabilizing locus for the widely varying pole and zero positions associated with variations in dynamic pressure (both below and above flutter). and for perturbations in their locations due to modeling errors.

The positions of the lightly damped complex conjugate zeros shown in Figure 4 arc critical in determining whether the root locus that occurs is stabilizing or nonstabilizing. These 'critical' zeros are also responsible for a relatively large gain required to stabilize the system using gain feedback. The large gain required for stabilization is undesirable mainly due to its potential effect on higher frequency dynamics. While the flutter mode can be stabilized, the large gain can easily cause higher frequency poles to become unstable. This was particularly problematic for the symmetric dynamics which have a secondary flutter mode.

Compensation elements were required to assure that the stabilizing root locus was achieved subject to plant variations and modeling errors and that the feedback gain could be small enough to assure that high frequency poles remain stable. Root locus concepts were used to develop a simple third-order filter structure that accomplished the stated objectives. The filter was characterized by a pair of complex conjugate poles near the 'critical' zeros, an associated pair of highly ddmped complex conjugate zeros, and a first-order washout filter. The filter transfer function structure is

$$\frac{u(s)}{y(s)} = K\frac{s}{s+p}\frac{(s+a+jb)(s+a-jb)}{(s+c+jd)(s+c-jd)} \qquad (1)$$

where u(s) is the output and y(s) is the inpu: to the filter.

The wash-out filler pole was chosen tc assure that undesired low frequency disturbances and measurement biases were sufficiently attenuated. The compiex conjugate poles were placed in locations near, but clearly to the left of, the 'critical' zeros. This assured that the resulting pole-zero interaction caused the desired stabilizing root locus path to be achieved, even when subjected to moderate plait variations and mcdeling errors. The complex conjugate zeros were placed well into the left half plane at a frequency slightly above that of the complex conjugate poles. The positions of the zeros were chosen to simultaneously maximize the gain and phase margins of tne system over a range of dynamic pressures.

The filter structure described above provided a simple control law that allowed the flutter mode to be stabilized. However, there were several conflicting design objectives (e.g., increasing flutter dynamic pressure, robustness to dynamic pressure variations. robustness to modeling errors. and control surface actuator limits) that had to be met for the control law to be successful. These objectives were met by modifying the pole

and zero placements. the filter gain, and by combining the effects of the TEO and TEI control surfaces. The pole and zero placements were chosen by a combination of root locus and Nyquist analyses. The gain values were chosen primarily by Nyquist analysis and simulation to equalize the positive and negative gain margins over a wide range of dynamic pressures. Gain scheduling could potentially have been used to improve performance and robustness at each dynamic pressure. This option was not pursued, however, since the added complexity was deemed unacceptable. A single gain value was used at all dynamic pressures.

The final set of FSS control law parameters that were used in the flutter suppression control laws are

$$K = 0.4871 \text{ (degree/g)},$$
$$p = 5,\ a = 40,\ b = 75,\ c = 7,\ d = 70 \qquad (2)$$

A frequency response plot of this filter is shown in Figure 5. Note that the control law resembles an inverted notch filter since it amplifies signals over a narrow frequency range. This characteristic allowed the unstable plant pole to be stabilized with a gain sufficiently small that higher order plant dynamics were not significantly affected. Note also that there is no roll-off in the filter. This characteristic was acceptable because the desired roll-off is provided by the first-order, 25 Hertz antialiasing filter and by the high frequency attenuation associated with the tip accelerometer response. The added roll-off afforded by the antialiasing filter is superimposed on the filter frequency response in Figure 5.

The same filter was used to suppress symmetric flutter regardless of whether or not the model was free to roll because the symmetric flutter behavior was independent of whether or not the roll brake was engaged. The same filter parameters were also used to suppress the antisymmetric flutter mode when the roll brake was on. This was possible because of the similarity of the flutter characteristics of the two flutter modes. Only the TEO surface was used in the symmetric control law. Both the TEO and TEI surfaces were used in controlling the antisymmetric flutter mode. In this case both pairs of trailing edge control surfaces were driven by the same control law command with a gain ratio of -0.25 as shown in the block diagram presented in Figure 6. This ratio was determined by parametric simulation studies to simultaneously maximize gain and phase margins.

Integration with Rolling Maneuver Controllers

The FSS control law was designed independently from the rolling maneuver controllers. However, issues associated with simultaneously performing flutter suppression and rapid rolling maneuvers were considered in the FSS design. The bandwidth required to perform rolling maneuvers was of scfficiently low frequency that the commands of the roll controllers could be treated as disturbances to the FSS control law. The controllers used to perform rapid rolling maneuvers had bandwidth requirements below 1 Hertz while the predicted flutter dynamics were at frequencies above 10 Hertz. The washout filter, included in the FSS control law structure to attenuate biases and low frequency disturbances. provided the required sttenuation.

A major concern was the potential for the two controilers to compete for control power. When a control surface reaches its deflection or rate limit. a closed-locp system which uses that surface effecdvely becomes instantaneously open-loop. If this situation occurs beyond the open-loop flutter point for sufficiently long periods of time, flutter may occur. However, if control is only lost or degraded momentarily, siability can be maintained.

Deflection limits were placed on the roll controller commands so that there would be sufficient control deflection capability for the FSS controller to perform its flight critical function. Rate limits could not be imposed in a similar manner, however, due to controller software and hardware constraints. As a result, the potential for rate limiting had to be addressed in the design of the FSS control law. Results from an analysis to assess the effects of rate limiting are presented in the next section. Fortunately, no severe problems emerged and the design did not require modification to allow rapid rolling maneuvers to be performed at dynamic pressures beyond the open-loop flutter point.

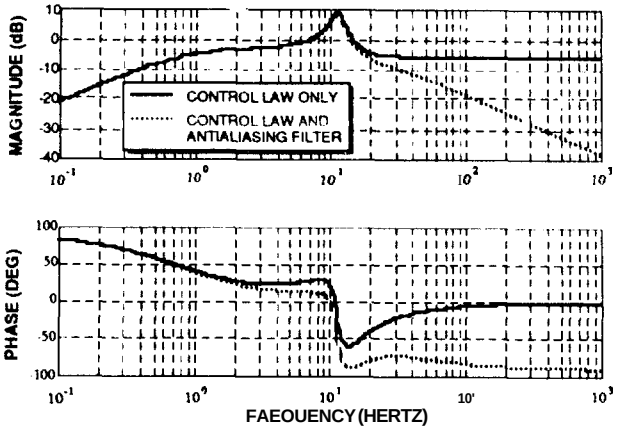

Figure 5 Control law frequency response (degree/g).

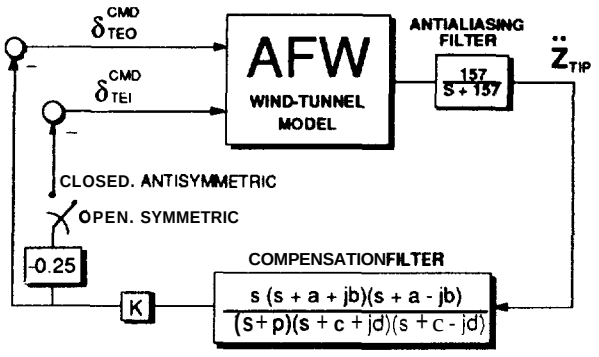

Figure 6 Control law block diagram.

Controller Performance and Discussion

Predicted Nominal Closed-Loop Performance

The predicted effect of applying the FSS controller to the nominal AFW wind-tunnel model is summarized in the closed-loop dynamic pressure root loci presented in Figures 7 and 8. The FSS control laws were predicted to stabilize both the symmetric and antisymmetric flutter modes to dynamic pressures in excess of 325 and 350 psf. respectively.

A comparison of the predicted open-loop and closed-loop dynamic pressure root loci reveals that the control law was able to suppress the primary flutter mode without affecting the higher frequency dynamics. The differences between the open-loop and closed-loop root loci are primarily restricted to the flutter region. Differences at higher frequencies are limited to minor perturbations. One notable difference between the open-loop and closed-loop root loci at high frequencies is the dynamic pressure at which a pole associated with the secondary symmetric flutter mode (at a frequency of about 35 Hertz) moves into the right half plane. In the open-loop case, the secondary flutter mode becomes unstable at a dynamic pressure of slightly over 350 psf while in the closed-loop case this occurs at a dynamic pressure between 325 and 350 psf. Since the maximum attainable dynamic pressure of the wind-tunnel was approximately 300 psf, no attempt was made to stabilize or otherwise affect the secondary symmetric flutter mode.

The predicted control surface activity required to achieve the desired level of flutter suppression was below the allowable maximum over a wide range of dynamic pressures. The predicted RMS control surface rate was below the specified maximum of 50 degrees per second over the range of dynamic pressure from 100 to 315 psf for the model fixed in roll. The

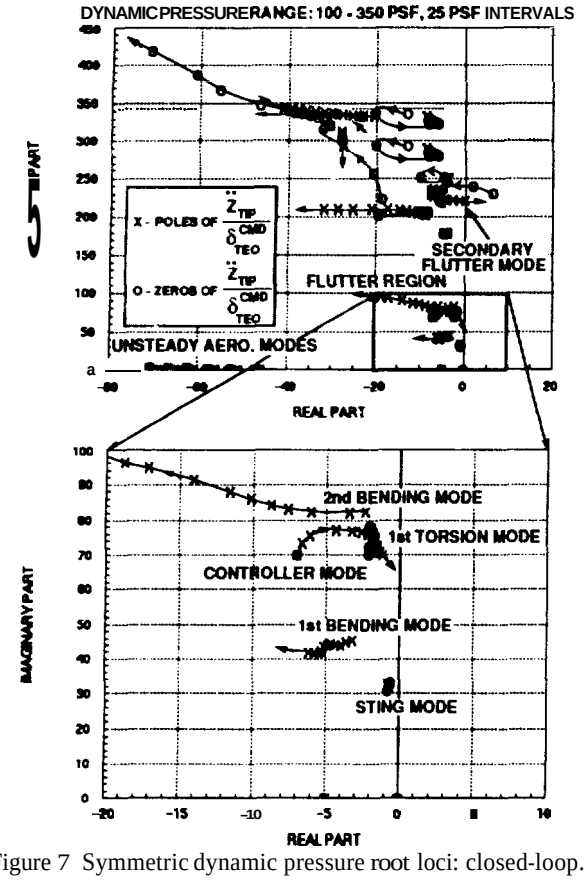

Figure 7 Symmetric dynamic pressure root loci: closed-loop.

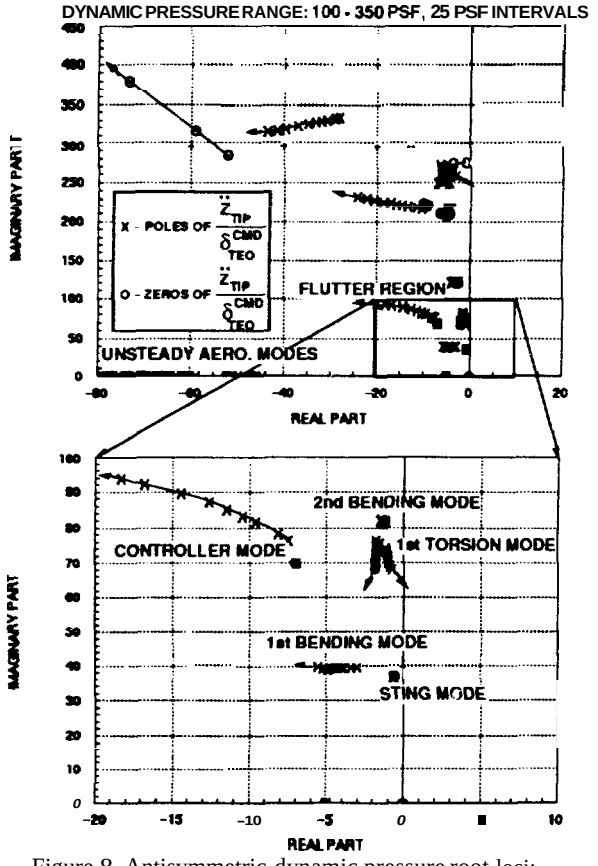

Figure 8 Antisymmetric dynamic pressure root loci: closed-loop (roll brake on).

predicted RMS control surface rate was below 50 degrees per second over the range of dynamic pressure from 100 to 300 psf for the model free to roll. The predicted RMS control surface rate required for the roll brake-off case at a dynamic pressure of 315 psf was slightly above 50 degrees per second.

Predictions of the symmetric and antisymmetric gain and phase margins for two sets of linear models are presented in Figure 9. The two models consisted of slightly different aerodynamic representations. Model 1 had a single aerodynamic lag associated with each structural mode to characterize unsteady effects. Model 2 had four aerodynamic lags and updated in vacuo vibration frequencies based on experimental data from a previous wind-tunnel test. The stability margins were computed by breaking the loop at the input to the controller (i.e., at the sensor channel).

The symmetric control law was single-input-single-output and so the gain and phase margins are accurate measures of robustness. The antisymmetric control law was single-input-multi-output and so the gain and phase margins were potentially nonconservative. However, since the control law was implemented so that both control surfaces received the same command (to within a constant factor of -0.25) and the uncertainties associated with the two control surface pairs are highly dependent, the effective single-loop margins were deemed acceptable. More general multivariable stability margin measures (e.g., minimum singular value of the inverse return difference matrix at the plant input) were conservative in this instance. They were computed, however, and given due consideration [Adams, et al. (1992)].

Both the symmetric and antisymmetric control laws satisfied the 14 dB gain margin specifications over a range of dynamic pressures from 100 to 325 psf. The 30 degree phase margin specifications were satisfied over a range of dynamic pressures from 100 to 350 psf with one exception. At dynamic pressures between 300 and 350 psf the negative symmetric phase margins were within 1 degree of the specification.

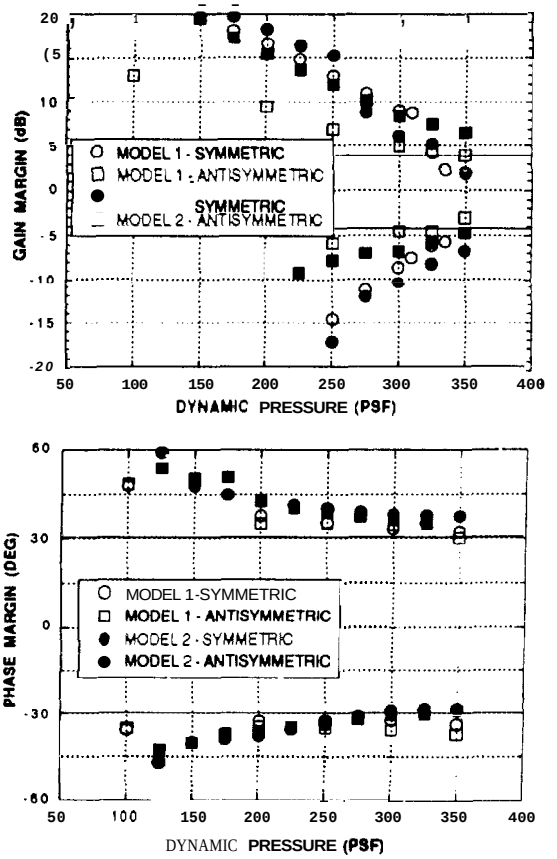

Figure 9 Predicted stability margins.

Table 1 - Sensitivity to Aeroelastic Frequency and Control Effectiveness - Symmetric Mode (Dynamic Pressure = 300 psf)

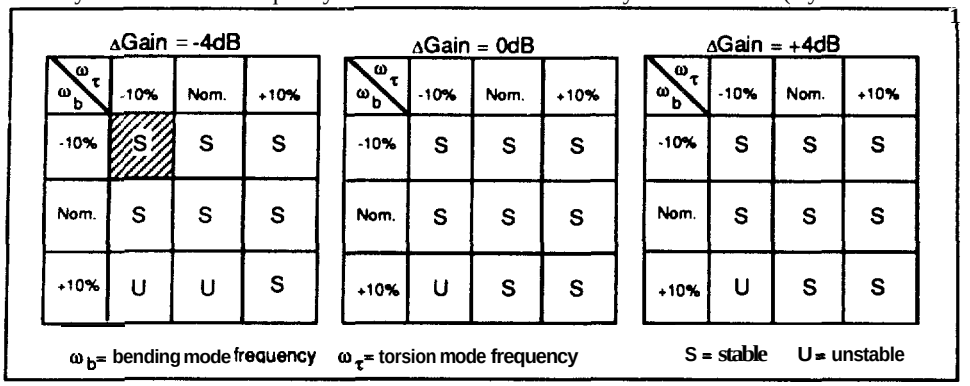

ΔGain = -4dB

ω_b \ ω_τ	-10%	Nom.	+10%
-10%	S	S	S
Nom.	S	S	S
+10%	U	U	S

ΔGain = 0dB

ω_b \ ω_τ	-10%	Nom.	+10%
-10%	S	S	S
Nom.	S	S	S
+10%	U	S	S

ΔGain = +4dB

ω_b \ ω_τ	-10%	Nom.	+10%
-10%	S	S	S
Nom.	S	S	S
+10%	U	S	S

ω_b = bending mode frequency ω_τ = torsion mode frequency S = stable U = unstable

Predicted Sensitivity to Modeling Errors

Sensitivity analyses were performed to address the impact of several forms of modeling error. Two analyses which had important implications for the success of the FSS control law will be discussed here. The first sensitivity analysis addressed the effects of uncertainties in control surface effectiveness and the aeroelastic frequencies of the two structural modes that led to flutter. The second sensitivity analysis addressed the effect of performing flutter suppression in combination with rapid rolling maneuvers.

The nonlinear simulation model was used to evaluate the Stability of the closed-loop system at a dynamic pressure of 300 psf subject to simultaneous variations in the frequencies of the two key aeroelastic modes and variations in control effectiveness. This was accomplished by separating the aerodynamic stiffness terms from the in vacuo vibration frequencies and perturbing the aerodynamic stiffnesses by ±10 percent. Variations in control effectiveness were approximated by varying control law gain by ±4 dB.

The results of this analysis applied to the symmetric dynamics are presented in Table 1. The results suggest that the symmetric controller was somewhat sensitive to a simultaneous increase in the bending mode frequency and decrease in the torsion mode frequency. The instability associated with the lower left hand matrix elements in Table 1 denotes this sensitivity. With the above noted exception, the controller was predicted to be robust to errors in the critical aeroelastic mode frequencies and control effectiveness.

The second sensitivity analysis was performed to assess the possibility that performing both flutter suppression and roll control might require more control activity than the actuators would be able to produce. The approach to assess possible interactions was to consider the impact of a worst case scenario as follows. The FSS control laws used the TEO surfaces as their primary control. The deflection limits imposed on the rolling maneuver controller commands were ±10 degrees. A typical rolling maneuver involved initiating a roll, sustaining it for a short period, and then stopping in less than 1.0 second from the time of initiation. Based on these factors, a worst case roll command (from the perspective of the FSS) was chosen to be a 10 degree doublet to the TEO surface with a period of about 1.0 second.

A simulation of the AFW wind-tunnel model was driven by the roll doublet and wind-tunnel turbulence while the FSS controller was operating at a dynamic pressure of 300 psf. Since the model was free to roll the antisymmetric control channel was open. Consequently, the FSS controller generated only symmetric commands whereas the roll controller generated purely antisymmetric commands.

During the simulated roll maneuver some rate limiting occurred. However, the limiting only affected one side of the AFW wind-tunnel model at each instant and only for very short periods of time on the order of 0.05 second. For comparison. the time to double amplitude of the flutter mode at a dynamic pressure of 300 psf is approximately 0.14 second. When the roll command required maximum control surface rate (to initiate or stop the roll), one TEO surface moved up and the other moved down at the rate limit. The symmetric flutter suppression controller simultaneously commanded control deflections that caused both TEO control surfaces (left and right) to move in the same direction. Therefore, the side that was commanded by both controllers to move in the same direction experienced rate limiting. The other surface, however, operated below the rate limit. The flutter suppression control law never became completely ineffective due to rate limiting. It did. however, momentarily loose some effectiveness since it was, in effect, only operating on one side of the vehicle at a time. As a result, some of the gain margin was "used up" during the period of rate limiting. The FSS controller had no difficulty maintaining system stability subject to the simulated worse case roll doublet.

Wind-Tunnel Test Results

Two wind-tunnel tests were performed using the FSS controller. The first test (Fall 1989) was aimed at performing plant estimation, flutter clearance tests, and validating the performance of active flutter suppression controllers and rolling maneuver controllers individually. The second test (winter 1991) was aimed at more extensive flutter suppression and rolling maneuver control tests, and validating the combination of flutter suppression and rolling maneuver control.

The FFS control law succeeded in suppressing the single symmetric flutter mode when the vehicle was free to roll and simultaneously suppressing two flutter modes (symmetric and antisymmetric) when the vehicle was fixed in roll. The flutter dynamic pressure was increased by over 24 percent when the model was fixed in roll and by over 23 percent when the model was free to roll.

In the fixed-in-roll case, oscillatory structural deflections caused loads that were in excess of preset safety limits. The excessive loads occurred at a dynamic pressure of 272 psf at which point testing was curtailed. The experimental data suggest that the controller stability limit had not been reached, the controller was providing sufficient damping to maintain stability. The oscillations, though sustained enough to exceed the safety limits, were stable.

In the free-to-roll case, the maximum dynamic pressure of the wind-tunnel (290 psf) was reached making further increases in dynamic pressure impossible. However, the FSS controller was performing as predicted. Extrapolation of the experimental data predicted that the dynamic pressure could have been increased to approximately 330 psf before closed-loop instability would occur. It should be noted. however, that safety limits would likely be exceeded before the stability limit could be attained, as was the case when the model was fixed in roll.

The control activity that was required to achieve the demonstrated levels of flutter suppression was less than half the design requirement. Figure 10 presents a comparison of the actual and predicted RMS control activity for the free-to-roll case. The peak RMS control rate was less than 15 degrees per second, which is well below the predicted level. This is an indication that the turbulence model used in the control synthesis was conservative at dynamic pressures above 200 psf. It is possible that higher gains could have been used to exploit the available control activity and improve controller performance. However, the gain values were based more on obtaining uniform stability margins than on limiting control

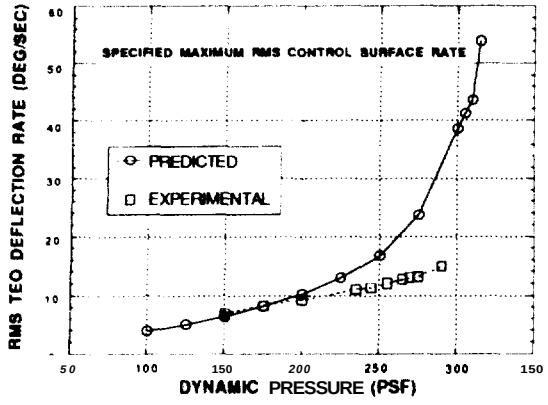

Figure 10 Comparison of control activity (roll brake off).

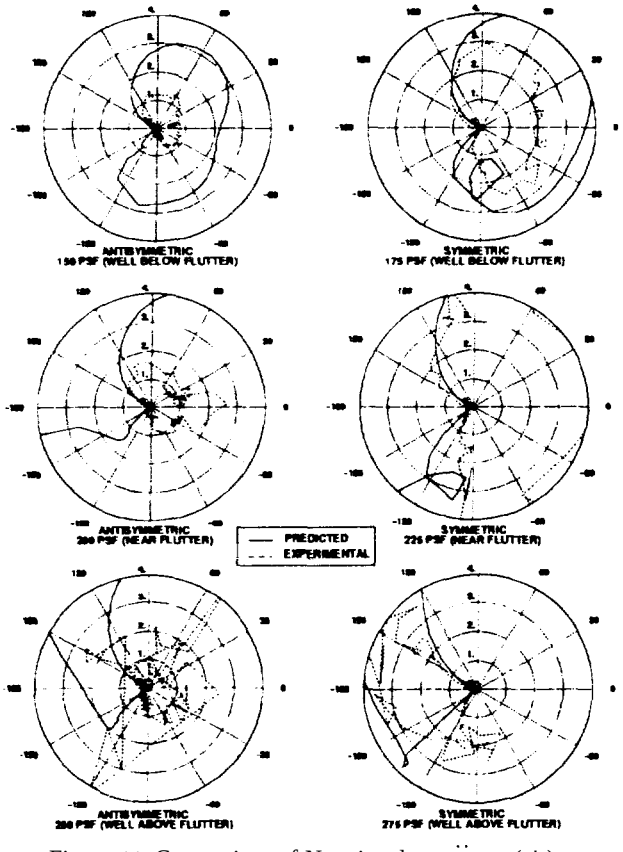

Figure 11 Comparison of Nyquist plots - $\ddot{z}_{TIP}$ (g's).

activity. Higher gains would also have led to smaller stability margins which would have been undesirable.

Another measure of performance of the FSS controller was the level of stability indicated by the Nyquist plots depicted in Figure 11. These plots were obtained from experimental data using the method described in Wieseman. et al. (1992) and Pototzky. et al. (1990). Plots for the symmetric AFW/FSS system at three dynamic pressures are presented: 175 psf. which is well below open-loop flutter; 225 psf, which is very close to open-loop flutter; and 275 psf, which is well beyond open-loop flutter. Plots for the antisymmetric AFW/FSS system at three dynamic pressures are also presented: 150 psf, which is well below open-loop flutter: 200 psf. which is very close to open-loop flutter; and 250 psf, which is well beyond open-loop flutter. Nyquist plots based on the mathematical model of the AFW wind-tunnel model are shown for comparison.

The demonstrated gain margins are well in excess of the ±4 dB required. The positive phase margins exceeded the requirement. but the negative phase margins were slightly smaller than -30 degrees. Some of the discrepancy between the predicted and actual phase margins can be attributed to the effects of digital implementation of the controller. The phase shift between the predicted and experimental results is almost entirely attributable to a time delay of one-half sample period, approximately 0.0025 second. The predicted Nyquist plots included an approximation of the effective time delay which was conservative by approximately one-half sample period.

The FSS controller was combined with a rolling maneuver controller [Moore, et al. (1992)] to demonstrate the ability to perform flutter suppression while performing rapid rolling maneuvers. The test involved performing rapid rolling maneuvers over a range of dynamic pressures both below and above flutter. At a dynamic pressure of 260 psf (25 psf beyond open-loop flutter). the rolling maneuver controller accomplished a 90 degree roll. starting from rest, in less than 0.5 second. The time to double amplitude of the flutter mode at this dynamic pressure was approximately 0.24 second. The flutter suppression controller had no difficulty maintaining stability during the rolling maneuver. The control activity and vehicle responses suggested no significant differences between the FSS performance in either steady or maneuvering flight.

Discussion

Plant identification was performed during both wind-tunnel tests. The experimentally determined open-loop flutter dynamic pressures were 235 and 219 psf for the symmetric and antisymmetric modes, respectively. The experimentally determined flutter frequencies were 9.6 and 9.1 Hertz for the symmetric and antisymmetric modes, respectively. The antisymmetric flutter mode data corresponds to the condition when the model was fixed in roll. Notice that the predicted values differ from those estimated using experimental data. The predicted flutter dynamic pressures were nonconservative in that they overpredicted the observed values. The error in the predicted flutter frequencies were 16.7 and 19.8 percent for the symmetric and antisymmetric modes. respectively.

Transfer functions for key input-output pairs at subcritical dynamic pressures (i.e. below flutter) were determined prior to closing the loop with the FSS controller. This allowed the control designers to study the accuracy of the design models and to assess the impact of modeling errors before. the FSS controller was used to suppress flutter. Similar transfer functions were determined after the control loops were closed to evaluate the accuracy of the model at post-flutter conditions using the method described in Wieseman, et al. (1992) and Pototzky, et al. (1990).

Figure 12 presents two representative transfer function plots for the tip accelerometer response due to antisymmetric TEO control surface deflection with the model fixed in roll. The analytical results correspond to the mathematical model obtained by linearizing the nonlinear simulation model at conditions consistent with the test data. The experimental data was obtained from the 1991 wind-tunnel test Figure 12(a) corresponds to a dynamic pressure of 150 psf. which is well below the flutter dynamic pressure. The plot in Figure 12(b) corresponds to a dynamic pressure of 225 psf, which is slightly above the actual flutter dynamic pressure.

In both cases there is general agreement, however, there are also notable differences between the experimental data and the analytical results. One of the most notable differences is the shift in the frequencies of the key aeroelastic modes. In Figure 12(b) the poles, which corresponded in vacuo to the first bending and first torsion modes, occur at frequencies below the predicted values. As a result, flutter occurred at a frequency approximately 1.8 Hertz lower than predicted. Similar discrepancies occurred for the symmetric responses [Waszak and Srinathkumar (1991)].

Another difference between the analytical and experimental frequency responses are the peak magnitudes. The differences near the flutter frequency vary from 3 to 10 dB over a range of dynamic pressure from 150 psf to 225 psf. As a result, the actual control effectiveness in the flutter frequency range was considerably less than what was predicted. This effect is clearly

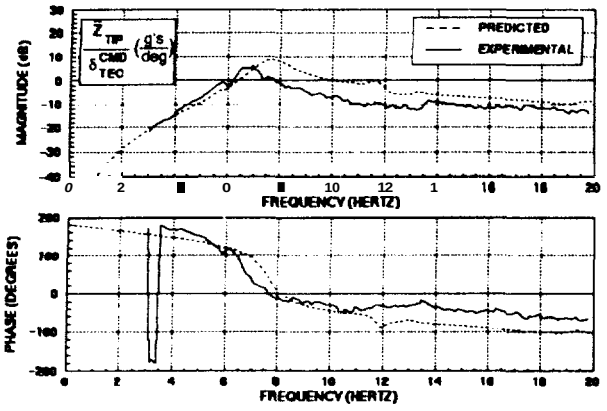

(a) Dynamic Pressure = 150 psf

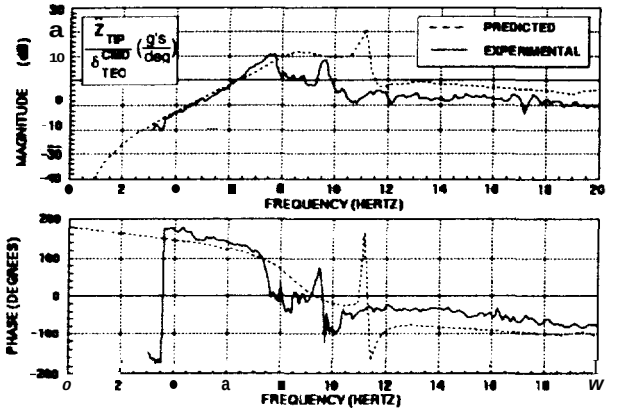

(b)Dynamic Pressure = 225 psf

Figure 12 Comparison of open-loop frequency responses - antisymmetric (roll brake on).

evident in the Nyquist plots for the antisymmetric AFW/FSS system shown in Figure 11. A similar effect is evident, but less pronounced, in the symmetric Nyquist plots.

The differences between the mathematical model and the actual vehicle were significant and a cause for concern. Fortunately. the FSS controller was robust to errors in both control effectiveness and aeroelastic mode frequencies, as shown in the results from the sensitivity analyses. The shaded region in Table 1 corresponds to simultaneous reduction in control effectiveness and reduction in bending and torsion mode aeroelastic frequencies.

Concluding Remarks

The Active Flexible Wing program demonstrated the feasibility of using active control systems to suppress flutter both in steady flight and while performing rapid rolling maneuvers representative of high performance military aircraft. These accomplishments were achieved despite errors in control effectiveness. flutter frequency, and flutter dynamic pressure in the design model, which nevertheless accurately characterized the flutter mechanism. The design approach exploited a fundamental understanding of the flutter mechanism and used a simple structure with inherent robustness properties and resulted in control laws that were relatively insensitive to observed modeling errors.

The future success of active flutter suppression depends to a large extent on the ability to generate accurate mathematical models. Accuracy requires not only good predictions of the flutter frequency, flutter dynamic pressure. and static control effectiveness, but also the *frequency* response properties of the vehicle over a wide range of dynamic pressures. In addition, many of the more advanced robust control methods require a characterization of the mathematical model uncertainty. Achieving the required level of accuracy and obtaining uncertainty representations will require continued research in the development of aerodynamic and structural modeling methods.

Regardless of the accuracy of the mathematical models, however. the control law designer must have a fundamental understanding of the flutter mechanism. Such an understanding reduces the potential for overly complex control laws that are difficult to implement or modify, control laws that interact with dynamic characteristics that have little role in influencing the key phenomena, and/or control laws which lack robustness to inevitable model errors. This study emphasizes the importance of developing a fundamental understanding of the dynamics, the importance of considering robustness to modeling errors in the control system design process. and the need for developing models that accurately characterize the physical phenomenon.

Acknowledgements

The authors wish to express their appreciation to Mr. Matthew J. Cummings for his efforts in obtaining the numerical results presented herein.

References

Adams. W.M.. Christhilf. D.M., Waszak, M.R., Mukhopadhyay, V.. and Srinathkumar. S.. "Design, Test, and Evaluation of Three Active Flutter Suppression Controllers," NASA TM-4338, 1992.

Bisplinghoff, R.L. and Ashley, H., *Principles of Aeroelasticity*, Dover Publications, Inc., New York. New York. 1975.

Buttrill, C.S., Bacon, B.J.. Heeg, J.. Houck. J.A., and Wood. D.. "Simulation and Model Reduction for the AFW Program," AIAA Paper No. 92-2081, Presented at the Dynamic Specialists Conference. Dallas, TX, April 16-17. 1992.

Buttrill, C.S. and Houck, J.A., "Hot-Bench Simulation of the Active Flexible Wing Wind-Tunnel Model," AIAA Paper No. 90-3121, September, 1990.

Hoadley. S.T.. and McGraw, S.M., "The Multiple-Function Multi-Input/Multi-Output Digital Controller System for the AFW Wind-Tunnel Model," AIAA Paper No. 92-2083, Presented at the Dynamic Specialists Conference. Dallas, TX, April 16-17.1992.

Moore, D.B., "Maneuver Load Control Using Optimized Feedforward Commands," AIAA Paper No. 92-2100, Presented at the Dynamic Specialists Conference, Dallas, TX, April 16-17, 1992.

Perry, B.. Cole, S.R.. and Miller, G.D., "A Summary of the Active Flexible Wing Program." AIAA Paper Number 92-2080. Presented at the Dynamic Specialists Conference, Dallas. TX, April 16-17,1992.

Pototzky, AS., Wieseman. C.D.. Hoadley, S.T.. and Mukhopadhyay. V., "Development and Testing of Methodology for Evaluating the Performance of Multi-Input/Multi-Output Digital Control Systems." NASA TM 102704, August 1990.

Schmidt, D.K. and Chen, T.K., "Frequency Domain Synthesis of a Robust Flutter Control Law," *Journal of Guidance and Control.* Vol. 9, No. 3. pp 346-351, May-June 1986.

Waszak, M.R. and Buttrill. C.S., "Design of an Active Flutter Suppression System for the Active Flexible Wing." AIAA Paper Number 91-3111, Presented at the AIAA Aircraft, Design, Systems, and Operations Meeting, Baltimore, MD. September 23-25, 1991.

Waszak. M.R. and Srinathkumar, S., "Active Flutter Suppression: Control System Design and Experimental Validation." AIAA Paper Number 91-2629, Resented at the AIAA Guidance, Navigation, and Control Conference. New Orleans, LA, August 12-14.1991.

Wieseman. C.D., Hoadley, S.T., and McGraw, S.M., "On-Line Analysis Capabilities Developed to Support the AFW Wind-Tunnel Tests," AIAA Paper No. 92-2084, Presented at the Dynamic Specialists Conference, Dallas, TX, April 16-17, 1992.

FLUTTER SUPPRESSION FOR THE ACTIVE FLEXIBLE WING: CONTROL SYSTEM DESIGN AND EXPERIMENTAL VALIDATION

AIAA-92-2097-CP

M.R. Waszak, *NASA Langley Research Center, Hampton, Virginia* *
Dr. S. Srinathkumar, *National Aeronautical Laboratory, Bangalore, India* **

Abstract

The synthesis and experimental validation of a control law for an active flutter suppression system for the Active Flexible Wing wind-tunnel model is presented. The design was accomplished with traditional root locus and Nyquist methods using interactive computer graphics tools and with extensive use of simulation-based analysis. The design approach relied on a fundamental understanding of the flutter mechanism to formulate a simple control law structure. Experimentally, the flutter suppression controller succeeded in simultaneous suppression of two flutter modes, significantly increasing the flutter dynamic pressure despite errors in the design model. The flutter suppression controller was also successfully operated in combination with a rolling maneuver controller to perform flutter suppression during rapid rolling maneuvers.

Introduction

Modem aircraft designs emphasize the reduction of structural weight to maximize efficiency and agility. Reduced structural weight. however. can result in reduced stiffness and may increase the likelihood of structural dynamic instabilities (flutter). Active flutter suppression is a possible solution to dynamic problems associated with reduced weight. Developing methods to suppress flutter by utilizing active control systems was one objective of the Active Flexible Wing (AFW) program [Perry, Cole and Miller **(1992)).**

This paper focuses on the design and wind-tunnel test of a control law for an active flutter suppression system (FFS). The operation of the flutter suppression controller with the AFW wind-tunnel model in a fixed attitude and while performing rapid rolling maneuvers are specifically addressed. An emphasis is placed on developing an understanding of the fundamental dynamic characteristics of the flutter mechanism and employing feedback in a manner that stabilizes the flutter mode without otherwise adversely affecting the basic dynamic properties of the wind-tunnel model and without undue complexity. Additional discussion of the design and validation of the control laws described herein is presented in Waszak and Srinathkumar (1991) and Waszak and Buttrill (1991).

Wind-Tunnel Model Flutter Characterization

Experimental Facilities

The AFW wind-tunnel model was an actively controlled, statically and aeroelastically scaled. full-span wind-tunnel model of an advanced fighter aircraft. The vehicle was supported by a sting with a ball bearing and brake mechanism that allowed the vehicle to be fixed or free to roll about the sting axis. Four control surfaces, controlled by hydraulic actuators, were located on each wing semispan: leading edge outboard (LEO), leading edge inboard (LEI), trailing edge outboard (TEO), and trailing edge inboard (TEI). Only three of these surfaces (LEO, TEI. and TEO) were utilized for flutter suppression. Four accelerometers were located on each wing semispan. Three of the accelerometers were located near the hingelines of the LEO. TEO and TEI control surfaces near the surface midspan and one was located near the wingtip at about midchord. A more detailed description of the wind-tunnel model is presented in Perry, Cole and Miller **(1992).**

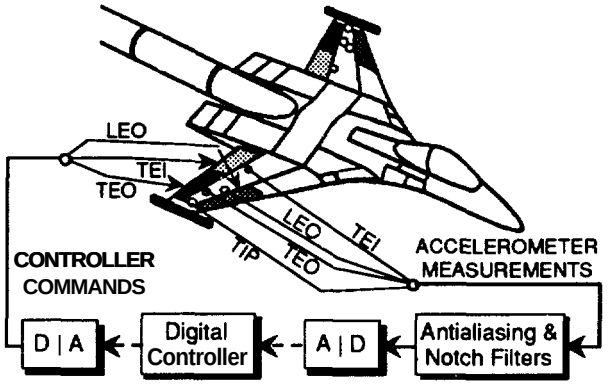

Figure 1 AFW wind-tunnel model and controller.

The active flutter suppression control law was implemented on a digital computer running at 200 samples per second. Analog measurement signals were prefiltered by a first-order. 25 Hertz antialiasing filter and could also be passed through notch filters. A schematic diagram of the AFW wind-tunnel model and controller is depicted in Figure 1. A detailed description of the digital controller is presented in Hoadley and McGraw **(1992).** The controller structure shown in Figure 1 could not be modified by the control law designer other than to specify characteristics of analog notch filters. Analog notch filters were not required for the control law described herein.

The wind-tunnel model and digital controller were tested during two wind-tunnel entries. These tests were performed in the NASA Langley Transonic Dynamics Tunnel (TDT). The operating conditions were limited to low subsonic speeds (< Mach **0.5)** at atmospheric pressure. Dynamic pressure was varied over a range from 0 to approximately 300 psf.

Mathematical Model

A high-fidelity simulation model of the AFW wind-tunnel model was used for control law synthesis and analysis. It consisted of representations of structural and aerodynamic characteristics. control surface actuator dynamics, wind-tunnel turbulence, and digital controller dynamics. Linear equations of motion for the structural dynamics, unsteady aerodynamics. and controller dynamics were used. but nonlinearities such as control surface deflection limits. actuator rate limits. and quantization effects were also characterized. The effects of wind-tunnel turbulence were incorporated into the model using an appropriately calibrated Dryden spectrum representation. A detailed description of the mathematical model can be found in Buttrill. et al. **(1992)** and Buttrill and Houck **(1990).** Linear models, used extensively in the control system design and analysis process, were obtained by linearizing the nonlinear model about equilibrium points at various operating conditions.

Flutter Mechanism

The predicted symmetric and antisymmetric dynamic characteristics of the AFW wind-tunnel model fixed in roll are summarized by the dynamic pressure root loci presented in Figures 2 and 3. The root loci describe the variation in pole and zero locations with variations in dynamic pressure of the open-loop transfer function associated with symmetric and antisymmetric tip accelerometer responses due to TEO actuator

* Aerospace Research Engineer, Member AIAA.
** Senior National Research Council Associate, NASA Langley Research Center. National Aeronautical Laboratory, Bangalore, India.